SEMARAK ILMU PUBLISHING

Journal of Advanced Research in Numerical Heat Transfer

Journal homepage:
https://semarakilmu.com.my/journals/index.php/arnht/index
ISSN: 2735-0142

CFD Modelling of Plasma Downdraft Coal Gasification Process: Effect of Throat Diameter on the Produced Syngas Composition

Muhammad Izhar Hishyam Anwari[1], Nor Afzanizam Samiran[2,*], Izuan Amin Ishak[1], Muhammad Suhail Sahul Hamid[3]

[1] Department of Mechanical Engineering Technology, Faculty of Engineering Technology, Universiti Tun Hussein Onn Malaysia, Pagoh Higher Education Hub, 84600, Muar, Johor, Malaysia
[2] Department of Mechanical Technology, Faculty of Mechanical and Manufacturing Engineering, Universiti Tun Hussein Onn Malaysia, 86400 Parit Raja, Batu Pahat, Johor, Malaysia
[3] ELS Energy and Lab Solutions Sdn. Bhd. No. 11A Tingkat Merpati Dua, Taman Transkrian 14300 Nibong Tebal, Pulau Pinang, Malaysia

ARTICLE INFO

Article history:
Received 22 April 2024
Received in revised form 20 May 2024
Accepted 21 June 2024
Available online 30 July 2024

Keywords:
CFD; Plasma gasification; Downdraft reactor; Coal; Throat diameter; Syngas

ABSTRACT

Plasma gasification is a high purity reaction which resulted on the conversion of carbon containing feedstock into syngas with extreme low tar content. Despite the advantages of low tar syngas, achieving high combustible component in syngas (H_2 and CO) via plasma gasification method through the modification of reactor was still unclear. Hence, the present study aims to investigate the effect of throat size of the plasma downdraft gasifier on the quality of produced syngas using Computational Fluid Dynamics (CFD) modelling. The effect of different sizes of reactor throat diameter on the temperature and produced syngas composition was systematically investigated and validated with previous study. The model geometry was developed by SolidWorks software package and simulation work was performed using Ansys Fluent software package. The design geometry of plasma throated downdraft gasifier involved a throat diameter of 201 mm, 164 mm, and 238 mm. The simulation model in this work was using the combustion, mixing and turbulent model of non-premixed combustion, Euler-Lagrangian method, and the K- turbulence model respectively. The Air, coal and plasma inlet temperature was set at 673 K, 293 K, and 1173 K, respectively. Whereas the air, feedstock and plasma gas flowrate were set at 0.0029 kg/s, 0.029 kg/s, and 0.0438 kg/s respectively. The results revealed that the throat diameter had a significant effect on the properties of the gas and temperature profile. This study reported that the temperature distribution at the centerline of reactor decreased with the increase of throat diameter. This result consequently caused the increase of the concentration of H_2, CO, and CH_4 by 8%, 12% and 6% due to the occurrence of endothermic reaction rather than exothermic reaction as complete combustion process is hindered.

1. Introduction

In the global trend of energy conservation and emission reduction, countries pay more attention to clean energy utilization technology, which is the key to reducing greenhouse gas emissions.

* *Corresponding author.*
E-mail address: afzanizamsamiran@gmail.com (Nor Afzanizam Samiran)

https://doi.org/10.37934/arnht.22.1.1430

Although coal resources are one of the largest pollutants, many countries still depend on coal for energy sources, liquid fuels in transportation and gaseous fuels for heating and chemical production. Coal is regarded as one of the dominant fuel sources throughout the 20th century globally. In 2018, 35.3 million metric tonnes of coal have been used in Malaysia where the majority of 92% was imported mostly from Indonesia (63%) and Australia (22%). There are two national energy policies including the National Energy Policy of 1979 and the fourth and fifth Fuel Policies, that drive the increasing coal usage in Malaysia [1]. Those policies program encourage the usage of coal to ensure a low-cost and dependable supply and lessen the reliance on oil by the energy sector. However, dependence on coal also presents a carbon balance problem in Malaysia. Despite the government's commitment to enhancing the usage of renewable energy, the share percentage of the total energy usage is still low due to technological difficulties. For example, the gasification of biomass technology poses some limitations due to its intrinsic properties of raw material such as high moisture content, low calorific value, high hydrogen content, hygroscopic nature, and low density, which makes it more crucial during transportation, storage, and preparation for gasification. Hence, this limitation caused the energy from biomass usage is yet unable to meet the energy demand brought by rapid economic development [2]. Consequently, limiting the pollutant emissions becomes challenging to protect the ecosystem from serious subsequences effect. Coal-based clean and efficient power generation technology is hence becoming a critical response in this instance.

One of the promising approaches to achieve clean coal usage is via coal gasification technology. Gasification is a partial oxidation process that converts carbonaceous materials into a clean syngas fuel (synthesis gas) which contained a combination of mostly H_2 and CO with minor quantities of CH_4, CO_2, N_2, char, ash, tar, and oils at temperatures between 973 and 1773 K [3]. The parameters such as type of gasifier, gasifying agent used (O_2, CO_2, air, or steam), equivalency ratio of the gasifying agent to the feedstock, and properties of feedstock attributed a significant impact on the percentage of components in the produced syngas [4]. Since the produced clean fuel of syngas can reduce the effect of greenhouse gas emission, gasification method is hence observed as highly potential technology for bio-waste disposal technology. The gasification process typically demonstrates a few conventional methods including downdraft, updraft, bubbling fluidized bed, circulating fluidized bed and entrained flow. The conventional gasification method also can be integrated with other elements such as heating element by plasma, gasifying agent of supercritical water, catalyst etc. to optimize the operability performance [5-7].

Plasma gasification has been used to decompose and eliminate hazardous pollutants by converting them into non-leachable slag. It has been observed as a valuable and effective process for solid waste treatment as the process produced lower gaseous emission. Hence, Plasma gasification is a promising method that can produce cleaner syngas due to a more efficient gasification process. Plasma is an electrified gas that exists in ions, free electrons and neutral particles that become electrically conductive when the gas atoms are energized by electric current or by producing high thermal energy [8]. The operation of plasma typically involves an electrical torch that can heat feedstocks to temperatures up to 1500°C which allows the disposal of solid waste. Plasma production also can be done with different setup of plasma torches, that consist of arc plasma (direct current (DC) transferred and non-transferred), radio frequency (RF), microwave, and inductively coupled plasma torches.

The implementation of plasma gasification for waste to energy conversion was still lacking with fundamental understanding through the experimental analysis. The complicated nature of the plasma process became a major factor that caused this task to be difficult to achieve. Currently, the growth in using numerical simulation method to understand the plasma gasification reaction has become an important part of designing the process [9]. Numerical simulation is known as one of the

viable analysis tools that can be used to predict and optimize the gasification performance of the process conversion, saving energy, material resources and time [9]. CFD methods are particularly useful for complicated solid conversion analysis and optimization, as well as for minimizing experimental difficulties by predicting statistical field values without impairing system operation [10]. A few works have been previously done on utilizing the computational fluid dynamics (CFD) approach to numerically investigate the behavior of the plasma gasification and to optimize the process. Beycan and Yilmazoglu conducted a 3D numerical simulation of plasma assisted downdraft gasification to investigate the effect of equivalence ratio (ER) on the produced syngas. The results reported that the lower heating value of syngas decreased from 1536.6 kcal/m3 to 751.8 kcal/m^3 as ER from 0.20 to 0.45 increase [11]. A.A. Erdogan and M.Z. Yilmazoglu conduct a numerical investigation via ANSYS Fluent software on the characteristic of medical waste gasification in updraft plasma gasifier. The results found that increasing the ER value enhance the production of H_2 and reduce the CO content in the syngas [12]. M. Sakhraji *et al.* suggested a simulation model of plasma gasification using MSW as feedstock to characterise the temperature distribution and the composition of produced syngas. The result found that plasma element was significantly affect the quality of syngas as the temperature distribution in the updraft gasifier operated at approximately 1000 K [13].

Previous study typically focused on the operating parameters such as equivalence ratio, temperature, and type of feedstock. However, investigation regarding the effect of reactor geometry on the performance of plasma gasification was rarely conducted. Due to the lack of studies that use CFD models for studying interaction between various design aspect of a gasifier geometry and operating conditions, the present study aim to propose an appropriate configuration of a throat size for plasma downdraft gasification as the attempt to produce high quality of syngas. The effect of varying the sizes of ratio of throat diameter to gasifier external diameter were numerically investigated using CFD simulation method.

2. Methodology

2.1 Reactor Geometry

A gasifier with a diameter of 371.86 mm and total heigh of 1366.8 mm as shown in Figure 1 was modelled in this study. The reactor consisted of three reaction zones including pyrolysis zone, oxidation zone and reduction zone. The throat of the gasifier was modelled for three different sizes of diameter which were 164 mm, 201 mm, and 238 mm (or equivalent with the ratios of throat to reactor diameter (d_T/D_R) of 0.44, 0.54 and 0.64). The different throat diameter is analyzed to investigate the effect of the design parameters on the syngas composition and temperature profile. The air inlet nozzles were created with a diameter of 30 mm at the center throat location of gasifier. The feeding inlet of feedstock was placed at the top of gasifier and the outlet nozzle was set at the 40 mm from the bottom side of the gasifier. This geometry was developed by using the parameters from the research carried out by Ibrahimoglu and Yilmazoglu [11]. This model was created using SolidWorks 2019 software package.

Table 1 illustrates the detail dimensions of throated downdraft gasification reactor with three different sizes of throat diameter. The throat diameter of 164 mm, 201 mm, and 238 mm were denoted as model 1, model 2 and model 3 respectively. Model 2 which represented as a middle size throat is treated as a baseline model to observe the effect of decreasing and increasing the size of throat which represented by model 1 and model 3 respectively.

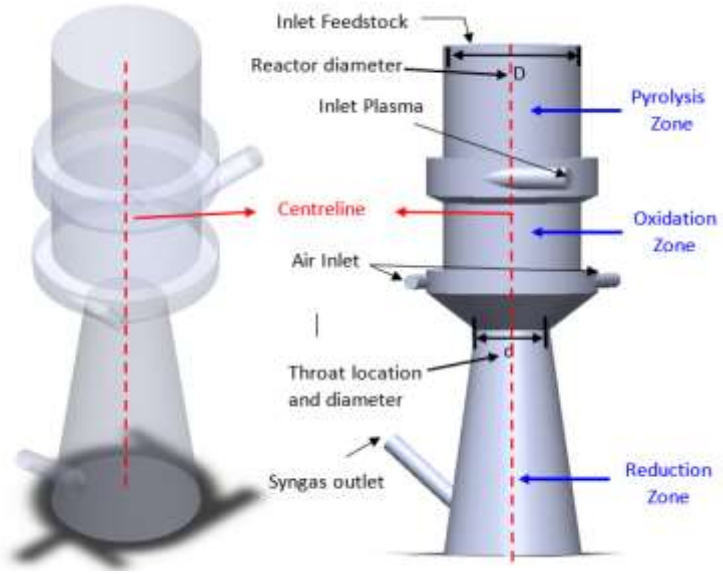

Fig. 1. 3D model of plasma downdraft gasifier [11]

Table 1
Dimension of reactor geometry with different sizes of throat diameter

Design Model 1	Design Model 2	Design Model 3
Throat diameter 164 mm (d_T/D_R= 0.44)	Throat Diameter 201 mm (d_T/D_R= 0.54)	Throat Diameter 238 mm (d_T/D_R= 0.64)
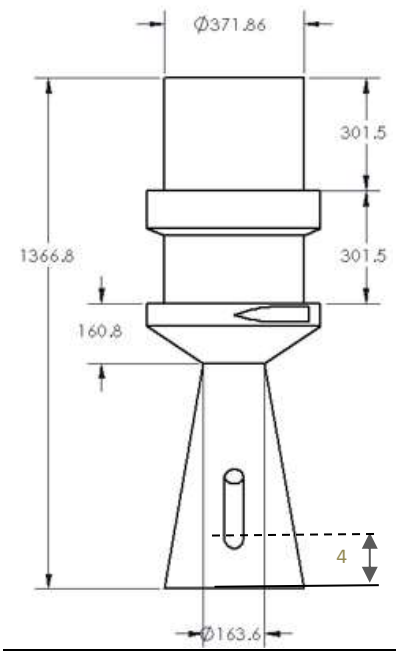	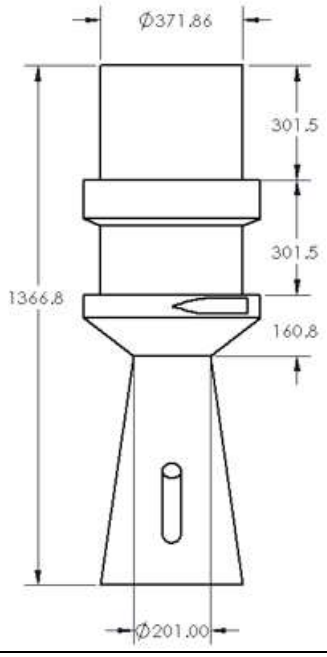	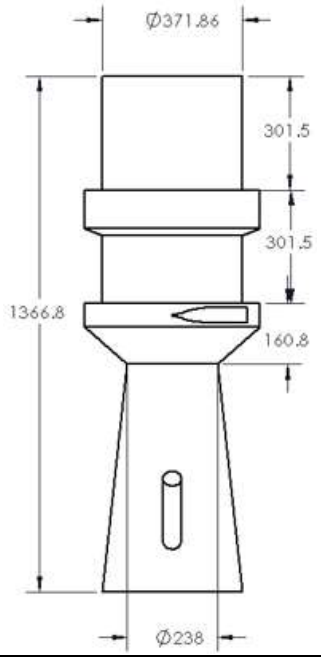

2.2 Computational Model

The present study used ANSYS FLUENT 19.0 software package to conduct the computational fluid dynamic (CFD) simulation analysis. The primary intention of the CFD study was to achieve accurate and reliable modelling results in an appropriate amount of computing time to allow the design optimization. Hence, the grid independence studies, convergence criteria and model validation were conducted to optimize the simulation computing time without interrupting the accuracy of the calculated parameters result. The species transport is solved under gravitational acceleration. The

Eulerian-Eulerian approach was used to solve transport phenomena, preserve momentum, mass, and energy equations. The gas phase turbulence flow within the gasifier was captured using the conventional k-ε model with normal wall functions. The SIMPLE algorithm scheme was used to fix the pressure-velocity coupling and standard system was used for discretion of the pressure.

2.2.1 Governing equation

The mass conservation equation, or continuity equation formulated as in Eq. (1)

$$\frac{\partial \mathrm{p}}{\partial \mathrm{t}}+\nabla\cdot(\rho\,\overrightarrow{\upsilon})=\mathrm{Sm} \tag{1}$$

Eq. (1) is the general form of the mass conservation equation, and it is valid for incompressible as well as compressible flows. The added mass due to the devolatilization of coal particles and vaporization of water droplets from secondary phase into the continuous phase is considered as the source, Sm. The momentum conservation equation, or conservation of momentum in an inertial (non-accelerating) reference frame is described by Eq. (2) [14,15].

$$\frac{\partial \mathrm{p}}{\partial \mathrm{t}}(\mathrm{p}\overrightarrow{\upsilon})+\nabla\cdot(\rho\ \overrightarrow{\upsilon}\ \overrightarrow{\upsilon})=-\nabla\mathrm{p}+\nabla\cdot(\overline{\overline{\tau}})+\rho\ \vec{g}+\vec{F}, \tag{2}$$

where p is the static pressure, τ is the stress tensor (described below), and $p\,\overrightarrow{g}$ and $\vec{F}$ are the gravitational body force and external body forces (for example that arise from interaction with the dispersed phase), respectively. $\vec{F}$ also contains other model-dependent source terms such as porous-media and user-defined sources. The stress tensor τ is given by Eq. (3):

$$\overline{\overline{\mathrm{t}}}=\mu\left[(\nabla\vec{v}+\nabla\vec{v}^{\mathrm{T}})-\frac{2}{3}\nabla\cdot\vec{\upsilon}\mathrm{I}\right] \tag{3}$$

where μ is the molecular viscosity, I is the unit tensor, and the second term on the right-hand side (RHS) is the effect of volume dilation. The energy conservation equation is described by Eq. (4):

$$\frac{\partial}{\partial \mathrm{t}}(\rho\mathrm{E})+\nabla\cdot\left(\overrightarrow{\upsilon}(\rho\mathrm{E}+\mathrm{p})\right)=-\nabla\cdot\left(\sum_{\mathrm{j}}\mathrm{h_j j_j}\right)+\mathrm{S_h}, \tag{4}$$

where $S_h$is the source term for particle-gas heat transfer, evaporation energy (latent heat), the radiation energy, and reaction heat.

2.2.2 Turbulence model

Transport equation for the standard k-ε transport equations for the turbulence kinetic energy, k, and its rate of dissipation, ε, are obtained from the following transport equations of Eq. (5) and (6) [11]:

$$\frac{\partial}{\partial \mathrm{t}}(\mathrm{pk})+\frac{\partial}{\partial \mathrm{x_i}}(\mathrm{pku_i})=\frac{\partial}{\partial \mathrm{x_j}}\left[\left(\mu+\frac{\mu_\mathrm{t}}{\sigma_\mathrm{k}}\right)\frac{\partial \mathrm{k}}{\partial \mathrm{x_j}}\right]+\mathrm{G_k}+\mathrm{G_b}+\rho\varepsilon-\mathrm{Y_M}+\mathrm{S_k}, \tag{5}$$

and

$$\frac{\partial}{\partial t}(\rho\varepsilon)+\frac{\partial}{\partial x_i}(\rho\varepsilon u_i)=\frac{\partial}{\partial x_j}\left[\left(\mu+\frac{\mu_t}{\sigma_\varepsilon}\right)\frac{\partial\varepsilon}{\partial x_j}\right]+C_{1\varepsilon}\frac{\varepsilon}{k}(G_k+C_3G_b)-C_{2\varepsilon}\rho\frac{\varepsilon^2}{k}+S_\varepsilon, \quad (6)$$

where S_k and S_ε are the source terms for k and ε respectively and $G_k$is the term to produce turbulent kinetic energy due to the mean velocity gradient and the Reynolds stress which defined as in Eq. (7):

$$G_k=-\rho\overline{u_i'u_j'}\frac{\partial u_j}{\partial x_i}, \quad (7)$$

G_b represents the generation of turbulent kinetic energy that arises due to buoyancy and is defined as Eq. (8),

$$G_b=\beta g_i\frac{\mu_t}{Pr_i}\frac{\partial T}{\partial x_i} \quad (8)$$

Y_M represents the contribution of the fluctuating dilatation in compressible turbulence to the overall dissipation rate and is defined as in Eq. (9):

$$Y_M=2\,\rho\varepsilon M_t^2 \quad (9)$$

The turbulent viscosity (μt) is computed by combining the local values of turbulent kinetic energy (k) and dissipation rate (ε) at each point by Eq. (10):

$$\mu=\rho C\,k\,\varepsilon \quad (10)$$

The values of $C1\varepsilon, C2\varepsilon, C\mu, \sigma k$ and $\sigma\varepsilon$ in Eq. (5) and (6) are constants and their values for the standard k-ε model are as follows:

$$C_{1\varepsilon}=1.44, \qquad C_{2\varepsilon}=1.92, \qquad C_\mu=0.09, \qquad \sigma_k=1.00, \qquad \sigma_\varepsilon=1.30$$

2.2.3 Reaction model

The reaction species model of non-premixed combustion model has been applied in this study as a solution to distinguish the mixture between feedstock and gasification medium. For each flow, the mass and momentum conservation equations were solved in Ansys-Fluent using Eq. (1) and Eq. (2). The energy conservation, depicted in Eq. (4), was useful in the non-adiabatic and non-premixed combustion model. The instantaneous thermochemical state of the fluid is linked to a conserved scalar variable known as the mixing fraction f under a series of simplifying assumptions, and this relationship forms the basis of the non-premixed modeling technique. The mixture fraction can be written in terms of the atomic mass fraction as Eq. (11):

$$f=\left(\frac{Z_i-Z_{i,ox}}{Z_{i,fuel}-Z_{i,ox}}\right) \quad (11)$$

2.2.4 Meshing model

The structure of mesh was generated by the mesh platform of Ansys workbench. The generated mesh covered all three zones in the reactor including pyrolysis zone, oxidation zone, and reduction

zone. The mesh parameter was set with a CFD physics environment, and the preferred linear element order and size for the fluent solver are 100mm. The type of generated mesh was unstructured tetrahedral mesh as depicted in Figure 2. The inflation was applied on the wall surface of reactor for calculation accuracy with the transition ratio of 0.272, minimum 5 layers and a growth rate of 1.2. The generated mesh on the reactor model comprises of 88409 elements which equivalence to 26173 nodes. The meshing quality in terms of skewness and orthogonality have averaged value of 0.23 and 0.79 respectively. Whereas orthogonal quality is determined to be 0.21 and 0.98.

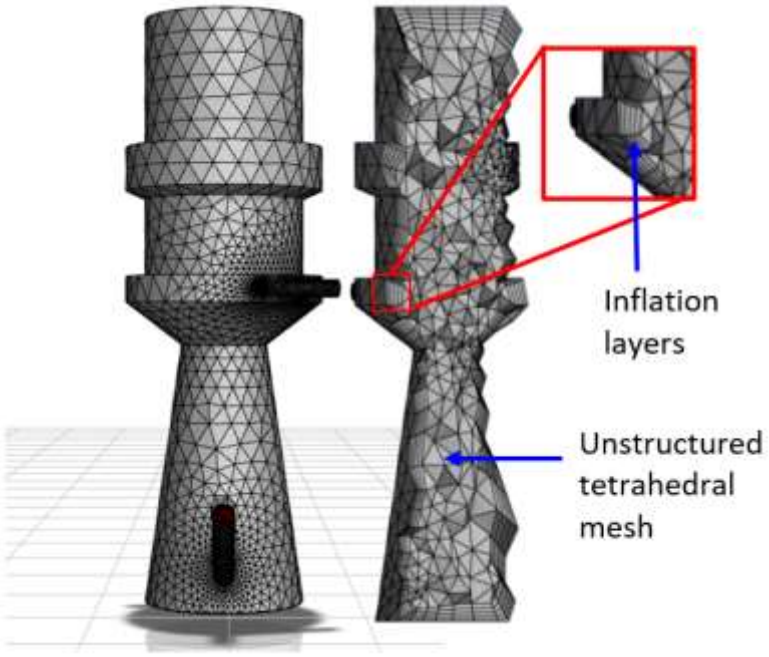

Fig. 2. Generated mesh of the reactor model

2.2.5 Boundary conditions

The simulation setup parameter was verified using the previous work which predominantly utilized coal as feedstock as shown in Table 2 [16]. The common setup of the boundary condition was including K-epsilon, energy, radiation, species movement, and Discrete Phase Model (DPM). The feedstock used in this study was coal. The properties of coal based on proximate and ultimate analysis were listed as in Table 3. The proximate analysis of coal is the process of defining the presence of different compounds and their amounts in coal including moisture content, volatile matter content, fixed carbon, and ash. Whereas ultimate analysis of coal is the process of determining different chemical elements that are present in coal including Carbon, C element, Hydrogen, H element, Oxygen, O, Sulphur, S and Nitrogen, N. The data of the composition of coal was based on I. Beycan and M.Z. Yilmazoglu [11].

A coal calculator features in the ANSYS Fluent solution setup is used to specify the proximate and ultimate properties of the coal. The proposed chemical kinetic scheme of gasification is also integrated into the species of non-premixed combustion. The inlet of air is selected as the mass-flow inlet and the gasifier outlet as the outflow. An adiabatic wall with the 'no-slip' condition is considered for the wall setup. The temperature of plasma was set at 1173 K. Coal and steam temperatures are 293 K and 673 K and mass flow rates of coal, plasma gas and air, are set to 0.029, 0.0438, and 0.0029 kg/s, respectively.

Table 2
The values of Reynolds number and velocity [16]

Type	Value or Description
Type of gasifier	Plasma gasification
System	Throat arrangement
Plasma temperature	1173K
Plasma flowrate	0.0438 kg/s
Feedstock type	Coal
Gasifier agent	Air
Gasifier agent flowrate	0.0029 kg/s
Feedstock flowrate	0.02908 kg/s
Turbulence model	K-epsilon

Table 3
Properties of coal based on proximate and ultimate analysis [11]

Properties of coal		
Category	Composition	Coal
Proximate analysis (wt. %, ar)	Ash, A	18.4
	Moisture, M	25.22
	Volatile, V	32.38
	Fixed carbon	23.55
Ultimate analysis (wt. %, ar)	Carbon, C	39.48
	Hydrogen, H	2.95
	Oxygen, O	12.83
	Nitrogen, N	0.59
	Sulphur, S	0.53
Lower heating value [kj/kg]	14248	

2.2.6 Solution method

The present study assumed the coal was fed from the top of the plasma gasification at a constant rate of 0.0438 kg/s and a temperature of 1173 K. The list of solution methods was depicted as in Table 4. The data of the solution method was adapted from P. Prasertcharoensuk *et al.* [4]. The solution method for turbulence model was using k-ɛpsilon model. The Semi-Implicit Method was used for Discretization (SIMD) Since Pressure-Linked Equations (SIMPLE) offers a benefit in the utilization of computer resources, it was employed. SIMPLE Scheme is selected to express the pressure-velocity coupling. All the spatial discretization was set to second order upwind, and gradient was set as least squares cell based.

2.2 Simulation procedure

The Computational Fluid Dynamic (CFD) simulation comprise a few designs stage and analysis including geometry development, meshing geometry, solver setup, simulation run and post-processing. The geometry model was developed using SolidWorks 2019 software package. The geometry model was then transferred to the workbench of ANSYS Fluent by using ANSYS Design Modeler. The mesh structure was then generated on the model. The setup of boundary condition was also defined during the meshing process including the selection of feedstock (coal) and gasifier agent (air) inlet and outlet of syngas. The simulation condition setup of meshed model was then

conducted in ANSYS Fluent solver. The gravitational force was utilized to act on the y-axis at -9.81m/s^2. The solver preference was set to use Fluent k-ε turbulence model and DO model for turbulence and radiation models. The properties of feedstock fuel, which in this case is coal, were set based on the proximate and ultimate analysis value as listed in Table 3. The species model was set to use non-premixed combustion model. The boundary condition of the inlet surface was defined as mass-flow inlet. The coal and steam temperatures were set at 293 and 673 K respectively. The mass flow rates of coal, plasma gas and air were set to 0.029, 0.0438, and 0.0029 kg/s respectively.

Table 4
List of setups for solution method [4]

Solution Method	Parameter
Pressure-velocity coupling	SIMPLE
Pressure	Standard
Gradient	Least Squares Cell Based
All other parameters	Second Order Upwind
Pressure	0.3
Density	1
Body Forces	1
Momentum	0.7
Turbulent kinetic energy	0.8
Turbulent viscosity	1
Energy	1
Temperature	1
Mean mixture fraction	1
Mixture fraction variance	0.9
Discrete phase sources	0.5
Initialization method	Hybrid initialization
Number of interactions	1500

3. Results

3.1 Grid Independence Study

Grid independence study was performed in this numerical analysis to determine the reliability of the meshing model. This stage is crucial as the parameters of simulation result is strongly dependence on the number, concentration, and quality of mesh. Hence, grid independence study is conducted to optimize the number of mesh, mesh type and mesh quality factors as to demonstrate an effective cost and time consuming yet high accuracy simulation results. Three different types of mesh have been generated for the grid independence study purposes and the detail of those meshing characteristics was listed as in Table 5. The orthogonality factor defined the ranges value from 0 to 1 as bad to good meshing quality. In contrast, the skewness factor demonstrated the reverse scale of ranges from 0 to 1 as good to bad meshing condition. Table 5 depicted that the obtained orthogonal maximum values were very close to 1 and skewness minimum values were very close to 0 which indicate that the cell is very close to being ideal [17]. This indicates that all types of generated meshing demonstrated a considerably good meshing quality.

The selection of appropriate meshing type was then conducted based on the selected parameter simulation results which in this case is average temperature values. Figure 3 indicates that meshing type with the element size of 100mm (88409 elements) and 70mm (92181 elements) demonstrated an identified results of temperature distribution. Hence, meshing size of 100mm has been chosen in this study as it reduces the calculation time and yet produced a comparable result with the meshing size of 70 mm which demonstrated higher number of element and meshing concentration.

Table 5
Generated mesh properties with different element size

No	Element size	Node	Element	Skewness	Orthogonal
1	70 mm	26173	92181	Min: 1.2299e-004 Max: 0.89899	Min: 0.10101 Max: 0.99143
2	100 mm	27124	88409	Min:1.3517 e-004 Max: 0.9	Min:0.1 Max: 0.99039
3	130 mm	25311	85037	Min: 1.0127e-004 Max: 0.89907	Min: 0.10093 Max: 0.98873

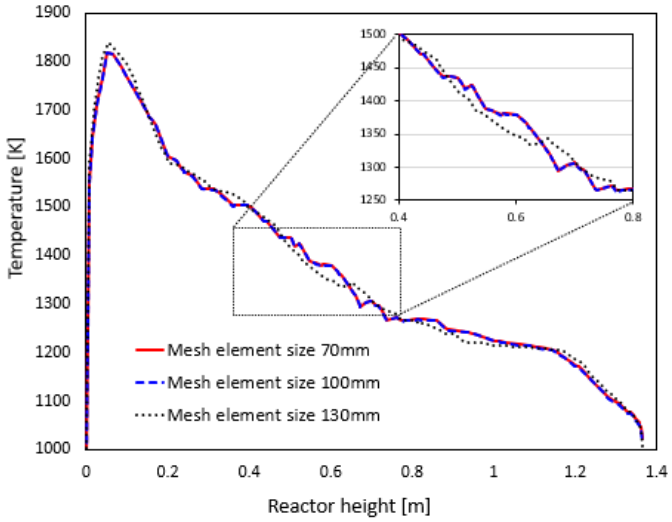

Fig. 3. Grid independence study for temperature against reactor height for different size of mesh

3.2 Convergence Criteria

Convergence criteria for any CFD simulation using ANSYS Fluent is typically based on the residuals of the equation being solved. The residuals are defined as a measure of the accuracy of the solution which continuously monitored during the simulation. The simulation of solving the equation is converge or reach a considerable accuracy of calculated results when the residuals value become slightly constant or steady state at certain number of iterations. Hence, convergence criteria can be used to evaluate the accuracy of the simulation. This criterion is based on the convergence of the solution to a steady-state solution. The criteria typically involve measuring the change in the model's parameters against number of iterations. The model's parameters are converged if the change is considered small enough. In this study, the convergence criteria were evaluated based on the value of methane (CH_4) compositions in the syngas as the measured parameter against the number of iterations. The iteration starts form 1000 iteration then increase to 1500 iteration and finally 2000 iterations. The simulation stops at the iteration number of 1650 that is considered converged as depicted in Figure 4.

3.3 Model Validation

The composition of produced syngas from the gasification process typically consists of carbon monoxide (CO), Hydrogen (H_2), Carbon Dioxide (CO_2), Methane (CH_4) and Nitrogen (N_2). Several parameters such as reactor geometry, gasifying agent, and types of feedstocks greatly influence the variations in the volume fraction of the syngas component. The present study established a

simulation model based on the previous study and parameters setup as listed in Table 2. The present model was then validated with the simulation model established by Ibrahimoglu and Yilmazoglu [11]. The deviation between the present result of carbon monoxide (CO), Hydrogen (H_2), Carbon Dioxide (CO_2), Methane (CH_4) and Nitrogen (N_2) with Beycan *et al.* was then assessed as depicted in Figure 5.

Figure 5 illustrated that the results of the present study were in good agreement with Beycan *et al.* as the average error percentage for all the syngas components was 12%. This average error percentage was identical with the value reported by M. Sharkaji *et al.* (12%) and close with A.A. Erdogan and M.Z. Yilmazoglu (8.6%) [12,13]. Both previous studies also conducted CFD simulation of plasma gasification. Hence, this model is considerably applicable to be used as a simulation model for the case study in this paper. The deviation was only 7%, 16%, 7%, 14%, 19% and 9% for CH_4, H_2, O_2, CO, CO_2, and N_2 respectively. The deviation of the present result seems to cause by the implementation of non-premixed combustion as a reaction species model rather than species transport model which used by Beycan *et al.* Since, the present study lacking with information from the previous study such as the value of injection through the discrete phase, non-premixed combustion model is hence decided to be use in this study which is a simplify to a mixing problem.

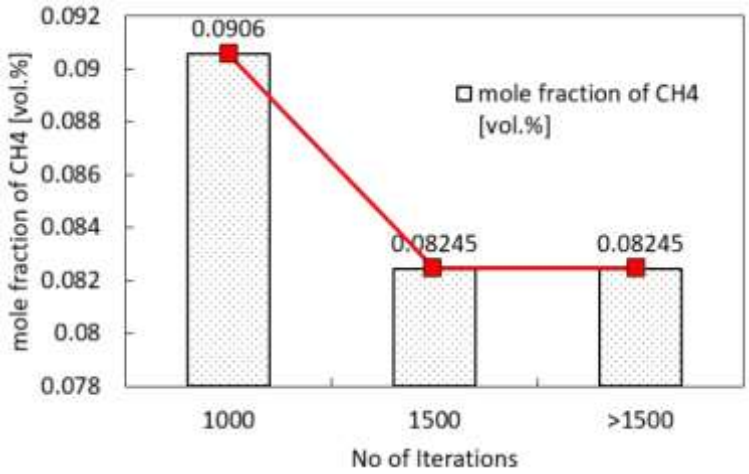

Fig. 4. Convergence criteria of CH_4 mole fraction against number of iterations.

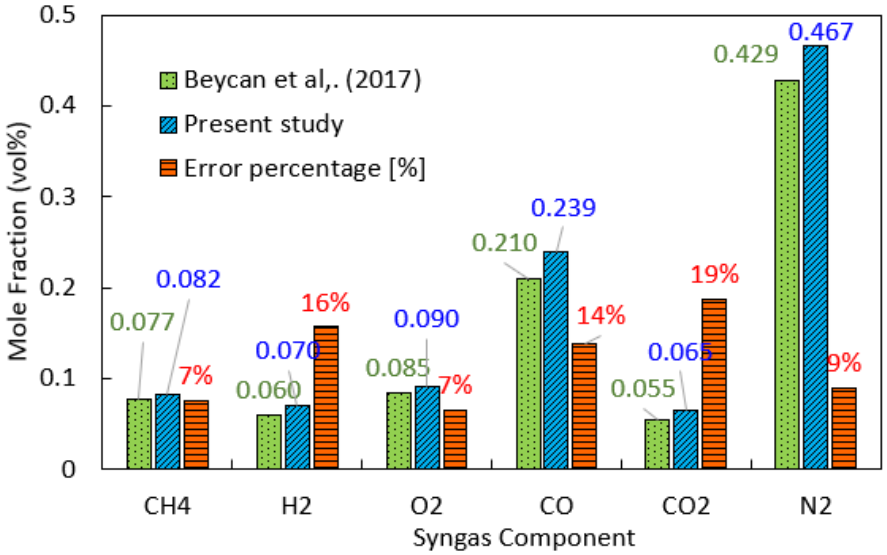

Fig. 5. Model validation of syngas mole fraction between present study with Ibrahimoglu and Yilmazoglu [11]

3.3 Temperature Distribution

Figure 6 shows the contour profile of the temperature distribution for the Model 1, Model 2, and Model 3. The result showed that the higher temperature distribution with dark red colour appearance was existed in a pyrolysis and oxidation zone and gradually decrease into reduction zone. The peak temperature or the ignition temperature of 1700 to 1850K was appeared close to the injection of plasma points. The temperature distribution was then decrease between 1200 to 1400K in the middle region of the gasifier. The result of temperature distribution contour also compared between model 1, 2 and 3. Figure 6 depicted that more region was covered with lower temperature region between 700 to 900K which appear in green colour for Model 2 with d_T/D_R= 0.54 and Model 3 with d_T/D_R= 0.64. This indicate that model 2 and 3 exhibited lower distribution of temperature within the reactor. In contrast, the reactor was entirely covered with temperature distribution of above 900K which appeared in light yellow colour for Model 1 with d_T/D_R= 0.44. This indicate that smaller throat diameter demonstrated higher temperature distribution within the reactor. The temperature distribution contour results also strongly agree with the plotted value of temperature at the centreline of reactor as depicted in Figure 7. Figure 7 showed that model 1 exhibited higher temperature distribution followed by model 2 and 3. However, model 3 demonstrated higher temperature distribution compared to model 2 especially at the region close to the top of reactor. This indicates that larger size of throat somewhat exhibits higher temperature distribution at certain region of reactor.

Since models 2 (201 mm) and 3 (268 mm) demonstrated wider region of lower temperature distribution, the gas stream in the reactor is expected to increase the amount of high molecular weight species (tar). However, model 1 (164 mm) yield higher temperature distribution in oxidation and reduction zone due to smaller size of throat which led to the high concentration of particle reaction. High and uniform temperature across the oxidation zone is important to eliminate tar formation in the gas stream [4].

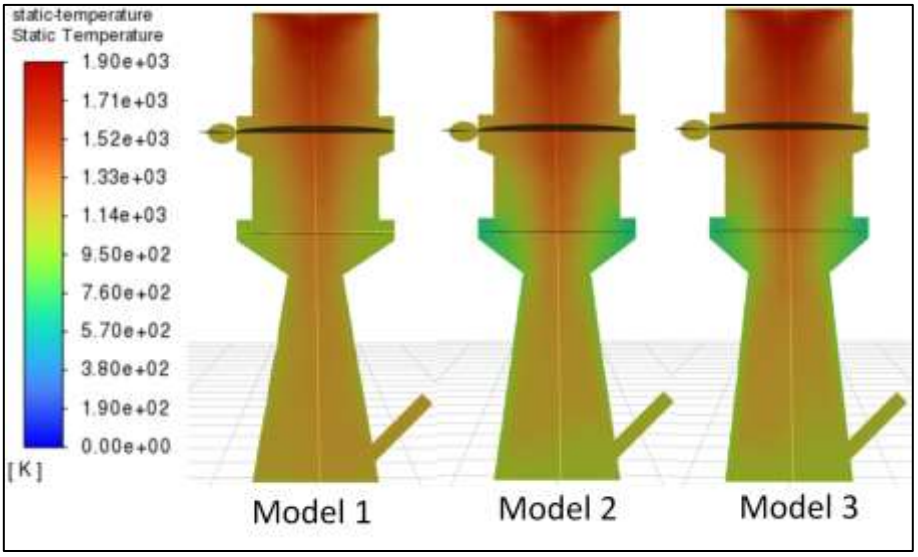

Fig. 6. Temperature distribution contour for model 1, 2 and 3

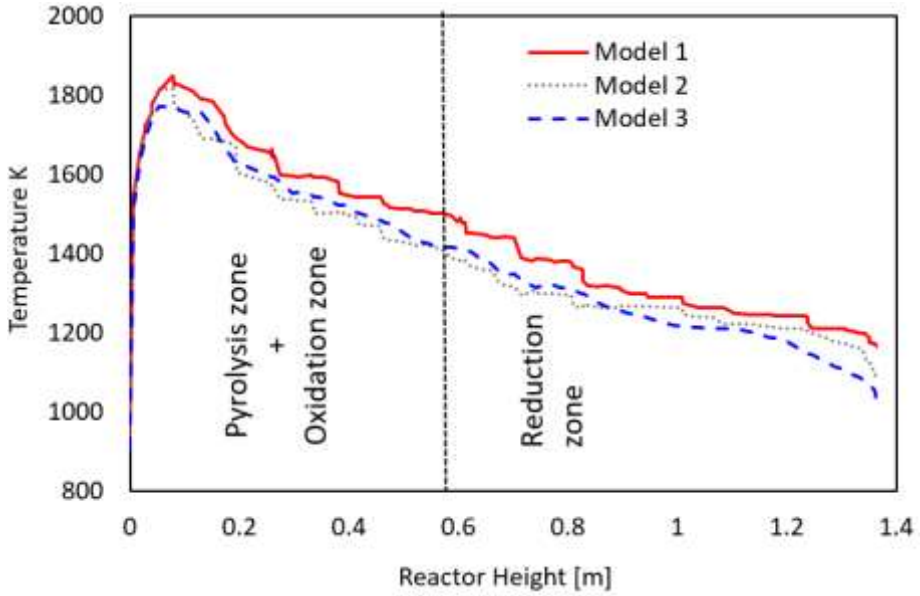

Fig. 7. Temperature against reactor height for model 1, 2 and 3

3.3 Syngas Composition Contour

Figure 8 depicted the species contour of CO component in syngas for model 1, 2 and 3. The concentration of CO content is increased up to 0.281% at top of the reactor. The species reaction that involved in producing CO was through oxidation and Boudouard reaction as formulated in Eq. (12), (13) and (14) [18-20].

$$C + 0.5O_2 \rightarrow CO,\ \triangle H^0 = -268\ kJmol^{-1} \quad (12)$$

$$C + O_2 \rightarrow CO_2,\ \triangle H^0 = -406\ kJmol^{-1} \quad (13)$$

$$C + CO_2 \rightarrow 2\,CO,\ \triangle H^0 = 172.6\ kJmol^{-1} \quad (14)$$

Figure 8 depicted that model 1 and 3 attributed more region covered with higher distribution of CO apparently right above the throat area which appeared in bright green colour compared to model 2. This indicate that larger and smaller size of throat diameter produced higher CO species compared to throat with middle size. This is implied with the results in Figure 6 and 7, where higher temperature distribution attributed by model 1 promoted higher exothermic reaction rate of oxidation as shown in Eq. (12) where the exothermic reaction of carbon, C component in raw material increase the production of CO. Whereas lower temperature distribution promoted endothermic reaction (absorbing heat) of Boudouard reaction as shown in Eq. (14) where the carbon, C component is more prone to incomplete reaction of producing CO rather than complete combustion to produce CO_2.

Figure 9 showed the contours of H_2 distribution for model 1, 2 and 3. The species reaction that involved in producing CO was through water-gas and water-gas shift reaction as formulated in Eq. (15) and (16),

$$C + H_2O \rightarrow CO + H_2,\ \triangle H^0 = 131.4\ kJmol^{-1} \quad (15)$$

$$CO + H_2O \leftrightarrow CO_2 + H_2,\ \triangle H^0 = -42\ kJmol^{-1} \quad (16)$$

The results show that the production of H_2 was insignificant as the region covered by the H_2 contour was least between those models. This indicate that the effect of throat diameter is unclear since the produced H_2 was low. However, it is visibly showed that model 3 and 1 seems exhibit a slightly wider region of H_2 contour compared to model 2. The distribution of CO and H_2 species were also generally exhibited a gradual decrease amount from the pyrolysis and oxidation zone into the reduction zone. This profile species distribution was also reported by Maya *et al.* [21]. L. Montuori *et al.* also reported that increasing the size of throat is relatively increase the produced amount of reactive gas in syngas [22].

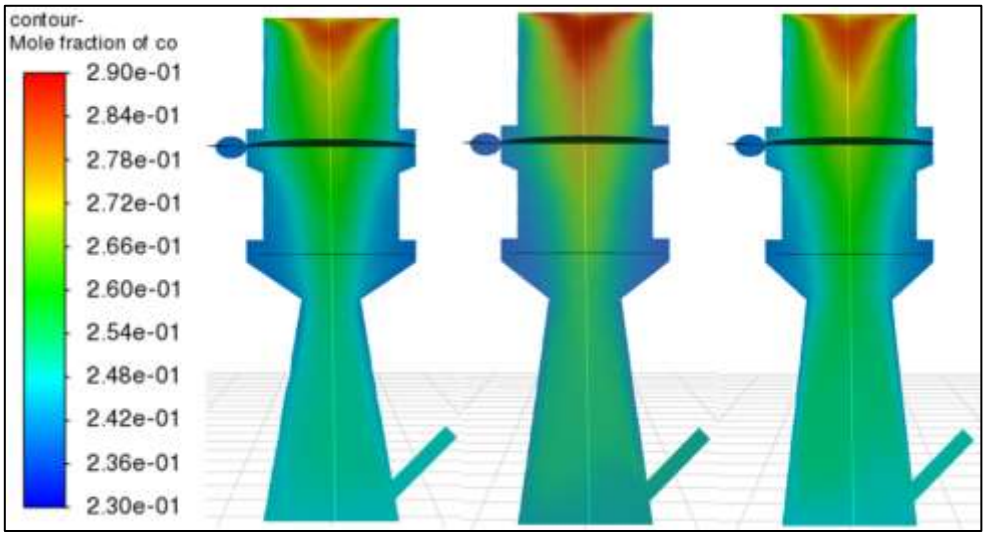

Fig. 8. Mole fraction of CO contour for model 1, 2 and 3

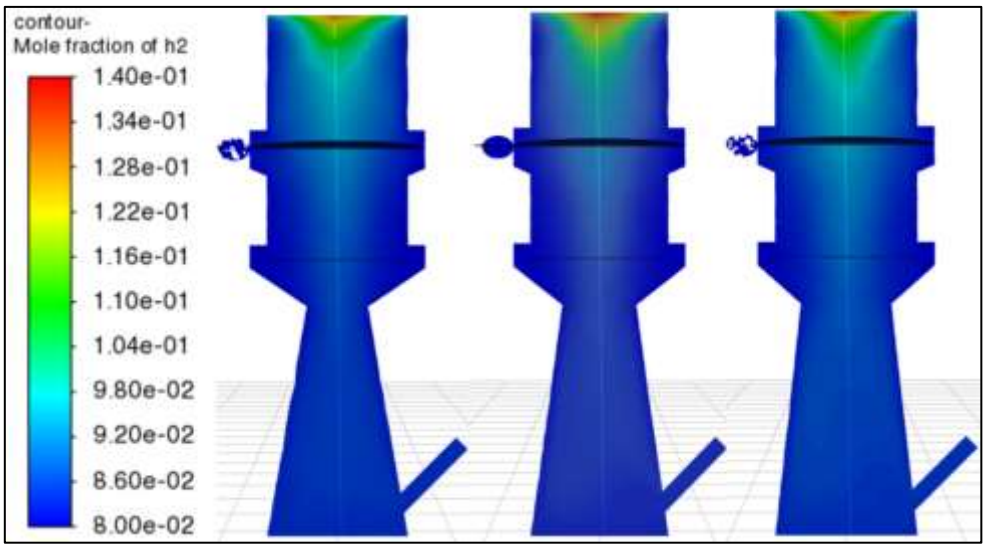

Fig. 9. Mole fraction of H_2 contour for model 1, 2 and 3

3.3 Syngas Composition at the Reactor Outlet

Figure 10 shows the species composition that produced at the outlet of the reactor for model 1,2 and 3. The result seems strongly corelated with the contour result of Figure 8 and 9 where the higher CO and H_2 composition was primarily produced by model 3 followed by model 1 and 2. The composition of CH_4 was also relatively higher for model 3. The composition of H_2, CO and CH_4 was increase by 8%, 12% and 6% using model 3 as compared to the lowest composition of model 2. This

implies that higher d_T/D_R ratio or larger size of throat diameter which attributes lower temperature distribution promotes higher endothermic reaction of boudouards, water-gas, and steam-reforming reaction (Eq. (14) and (15)) which resulted on the high production of H_2, CO and CH_4 species. This trend of increasing combustible component in syngas with the increase of throat diameter was also reported by Bunchan *et al.,* [23]. Smaller size of throat diameter somewhat also produced higher H_2, and CO composition compared to middle size of throat diameter. Higher distribution temperature attributed by model 1 also can be a factor to produce higher syngas composition through exothermic reaction of partial oxidation and water gas shift reaction (Eq. (12) and (16)).

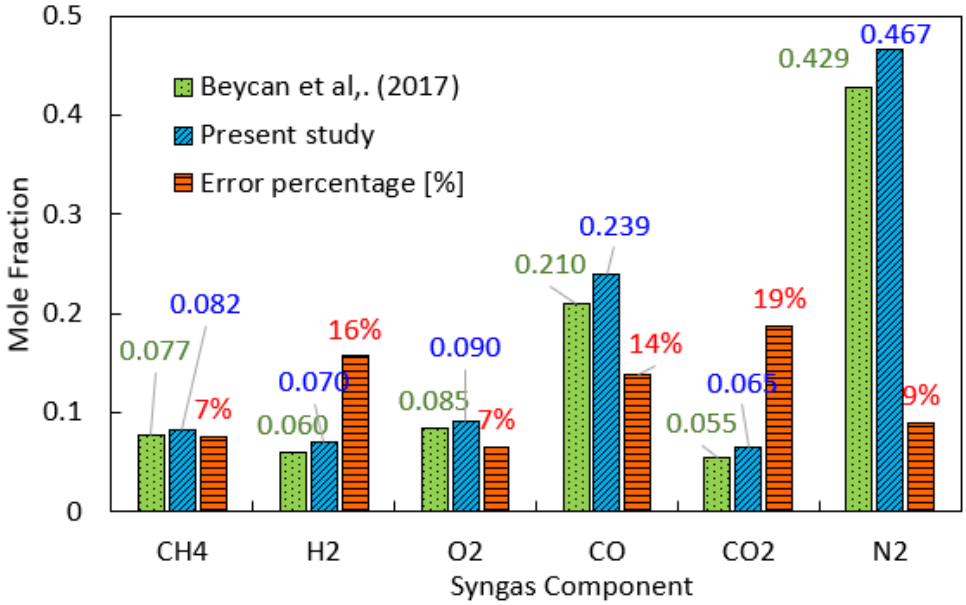

Fig. 10. Mole fraction of syngas composition for model 1, 2 and 3

4. Conclusions

The present study conducted a 3D numerical CFD simulation analysis of plasma coal gasification using downdraft reactor to study the effect of throat diameter on the produced syngas. The applied simulation model was first validated with previous study by comparing the composition of syngas component with the same setup of throat diameter size and type of feedstock. The present result was in good agreement with the previous study as the percentage error was considerably lower and accepted for further analysis of simulation study. The validated simulation model was then used for analysis of coal plasma gasification using three different size of throat diameter or throat to reactor diameter of d_T/D_R= 0.44, 0.54 and 0.64 denoted as model 1, 2 and 3. The result of temperature distribution indicate that increasing the d_T/D_R resulted on the decrease of temperature distribution. This implies that lower and higher d_T/D_R which specifically referred to model 1 and 3 produced higher and lower temperature distribution which relatively can increase the rate of exothermic and endothermic reaction respectively. The present simulation results also showed that different size of throat poses a significant effect on the syngas composition and temperature distribution particularly in the oxidation zone and pyrolysis zone. Higher d_T/D_R attempt to increase the composition H_2, CO, and CH_4 by 8%, 12% and 6% as compared to model 2 which produced the lowest composition of those gas component.

Acknowledgement

This research was supported by Universiti Tun Hussein Onn Malaysia (UTHM) through Tier 1 (vot Q393).

References

[1] Nicole Fong. *Rise of Coal in Malaysia*. 2021 [cited 2022; Available from: https://www.macaranga.org/coal-statistics-malaysia/.

[2] Alka D. Kamble, Vinod Kumar Saxena, Prakash Dhondiram Chavan, and Vinod Atmaram Mendhe. "Co-gasification of coal and biomass an emerging clean energy technology: Status and prospects of development in Indian context." *International Journal of Mining Science and Technology* 29, no. 2 (2019): 171-186. https://doi.org/10.1016/j.ijmst.2018.03.011

[3] Qing He, Qinghua Guo, Kentaro Umeki, Lu Ding, Fuchen Wang, and Guangsuo Yu. "Soot formation during biomass gasification: A critical review." *Renewable and Sustainable Energy Reviews* 139 (2021): https://doi.org/10.1016/j.rser.2021.110710

[4] Phuet Prasertcharoensuk, David A. Hernandez, Steve J. Bull, and Anh N. Phan. "Optimisation of a throat downdraft gasifier for hydrogen production." *Biomass and Bioenergy* 116 (2018): 216-226. https://doi.org/10.1016/j.biombioe.2018.06.019

[5] Weizuo Wang, Qiuyang Zhao, Bingru Lu, Jinwen Shi, and Hui Jin. "Pure hydrogen gas production in a coal supercritical water gasification system with CO2 as transporting medium." *Applied Thermal Engineering* 237 (2024): https://doi.org/10.1016/j.applthermaleng.2023.121529

[6] Samy Yousef, Andrius Tamošiūnas, Mindaugas Aikas, Rolandas Uscila, Dovilė Gimžauskaitė, and Kęstutis Zakarauskas. "Plasma steam gasification of surgical mask waste for hydrogen-rich syngas production." *International Journal of Hydrogen Energy* 49 (2024): 1375-1386. https://doi.org/10.1016/j.ijhydene.2023.09.288

[7] Nazlıcan Yesilova, Ozgun Tezer, Atakan Ongen, and Azize Ayol. "Enhancing biomass gasification: A comparative study of catalyst applications in updraft and modifiable-downdraft fixed bed reactors." *International Journal of Hydrogen Energy* (2024): https://doi.org/10.1016/j.ijhydene.2024.05.075

[8] Kaushal, Rajneesh, Rohit, and Amit Kumar Dhaka. "A comprehensive review of the application of plasma gasification technology in circumventing the medical waste in a post-COVID-19 scenario." *Biomass Conversion and Biorefinery* 14, no. 2 (2024): 1427-1442. https://doi.org/10.1007/s13399-022-02434-z

[9] Ismail, Tamer M., Eliseu Monteiro, Ana Ramos, M. Abd El-Salam, and Abel Rouboa. "An Eulerian model for forest residues gasification in a plasma gasifier." *Energy* 182 (2019): 1069-1083. https://doi.org/10.1016/j.energy.2019.06.070

[10] Diba, Mst Farhana, Md Rezwanul Karim, and Jamal Naser. "CFD modelling of coal gasification in a fluidized bed with the effects of calcination under different operating conditions." *Energy* 239 (2022): 122284. https://doi.org/https://doi.org/10.1016/j.energy.2021.122284

[11] Ibrahimoglu, Beycan, and M. Zeki Yilmazoglu. "Numerical modeling of a downdraft plasma coal gasifier with plasma reactions." *International Journal of Hydrogen Energy* 45, no. 5 (2020): 3532-3548. https://doi.org/10.1016/j.ijhydene.2018.12.198

[12] Erdogan, Altug Alp, and Mustafa Zeki Yilmazoglu. "Experimental and numerical investigation of medical waste disposal via plasma gasification." *Applied Energy* 353 (2024): 122014. https://doi.org/https://doi.org/10.1016/j.apenergy.2023.122014

[13] Mariam Sakhraji, Ana Ramos, Eliseu Monteiro, Khalid Bouziane, and Abel Rouboa. "Plasma gasification process using computational fluid dynamics modeling." *Energy Reports* 8 (2022): 1541-1549. https://doi.org/10.1016/j.egyr.2022.08.069

[14] Murugan, P. C., and S. Joseph Sekhar. "Species–Transport CFD model for the gasification of rice husk (Oryza Sativa) using downdraft gasifier." *Computers and electronics in agriculture* 139 (2017): 33-40. https://doi.org/10.1016/j.compag.2017.05.004

[15] Ming-Hong Chen, Yau-Pin Chyou, and Ting Wang. "Simulation of Coal Gasification in a Low-Temperature, High-Pressure Entrained-Bed Reactor with a Volatiles Condensation and Re-Evaporation Model." *Applied Sciences* 9, no. 3 (2019): https://doi.org/https://doi.org/10.3390/app9030510

[16] Beycan Ibrahimoglu, Ahmet Cucen, and M. Zeki Yilmazoglu. "Numerical modeling of a downdraft plasma gasification reactor." *International Journal of Hydrogen Energy* 42, no. 4 (2017): 2583-2591. https://doi.org/10.1016/j.ijhydene.2016.06.224

[17] A. Iranzo, B. Toharias, C. Suarez, F. Rosa, and J. Pino. "Dataset and mesh of the CFD numerical model for the modelling and simulation of a PEM fuel cell." *Data Brief* 41 (2022): 107987. https://doi.org/10.1016/j.dib.2022.107987

[18] Pulla Rose Havilah, Amit Kumar Sharma, Gopalakrishnan Govindasamy, Leonidas Matsakas, and Alok Patel. "Biomass Gasification in Downdraft Gasifiers: A Technical Review on Production, Up-Gradation and Application of Synthesis Gas." *Energies* 15, no. 11 (2022): https://doi.org/https://doi.org/10.3390/en15113938

[19] Amira Nemmour, Abrar Inayat, Isam Janajreh, and Chaouki Ghenai. "Syngas production from municipal solid waste plasma gasification: A simulation and optimization study." *Fuel* 349 (2023): https://doi.org/10.1016/j.fuel.2023.128698

[20] Kuo, Po-Chih, Biju Illathukandy, Wei Wu, and Jo-Shu Chang. "Plasma gasification performances of various raw and torrefied biomass materials using different gasifying agents." *Bioresource technology* 314 (2020): 123740. https://doi.org/10.1016/j.biortech.2020.123740

[21] Maya, Diego Mauricio Yepes, Electo Eduardo Silva Lora, Rubenildo Vieira Andrade, Albert Ratner, and Juan Daniel Martínez Angel. "Biomass gasification using mixtures of air, saturated steam, and oxygen in a two-stage downdraft gasifier. Assessment using a CFD modeling approach." *Renewable Energy* 177 (2021): 1014-1030. https://doi.org/10.1016/j.renene.2021.06.051

[22] Lina Montuori, Carlos Vargas-Salgado, and Manuel Alcázar-Ortega. "Impact of the throat sizing on the operating parameters in an experimental fixed bed gasifier: Analysis, evaluation and testing." *Renewable Energy* 83 (2015): 615-625. https://doi.org/10.1016/j.renene.2015.04.068

[23] Bunchan, Sungwarn, Tinnakorn Poowadin, and Kittichai Trairatanasirichai. "A study of throat size effect on downdraft biomass gasifier efficiency." *Energy Procedia* 138 (2017): 745-750. https://doi.org/10.1016/j.egypro.2017.10.213